J. Fluid Mech. (1985), *vol.* 161, *pp.* 139–159
Printed in Great Britain

The use of flush-mounted hot-film gauges to measure skin friction in unsteady boundary layers

By A. N. MENENDEZ
Laboratorio de Hidraulica Applicada, INCYTH,
Buenos Aires, Argentina

AND B. R. RAMAPRIAN†
Department of Mechanical Engineering and Institute of Hydraulic Research,
The University of Iowa, Iowa City, Iowa 52242

(Received 18 May 1984 and in revised form 3 June 1985)

Flush-mounted hot-film gauges have proved very effective in measuring skin friction in steady laminar and turbulent boundary-layer flows. Their use is based on the analogy between momentum and heat transfer in the boundary layer. An extension of this technique for use with unsteady flows is presented, through the formulation of a more general relationship between the rates of heat and momentum transfer at the wall. The accuracy of the new formula and the range of its applicability are examined for the case of a periodic boundary layer, both in the laminar and turbulent regimes. This is accomplished by comparing the formula against exact numerical solutions of the differential equations. The present extension allows one to apply the hot-film technique to general unsteady-flow situations, including the measurement of the spectral density of wall-shear-stress fluctuations in steady turbulent flows.

1. Introduction

The technique of measuring wall shear stress in boundary-layer flows using flush-mounted hot-film gauges has been well established, to the point that these gauges are now available commercially. The gauge consists of a thin metallic film baked onto a non-conducting substrate (figure 1). The film forms one arm of a constant-temperature anemometer bridge. An electric current is passed through the film by a high-gain feedback amplifier so as to maintain it at a *constant* temperature, higher than the ambient fluid temperature, while heat is continuously being transferred from the film to the fluid. If the flow is steady and laminar, and the longitudinal pressure gradient negligible, the resulting heat-transfer rate Q_T to the fluid can be shown to be related to the wall shear stress τ_w as

$$\tau_w \propto Q_T^3. \tag{1}$$

The technique can also be applied to determine the time-mean wall shear stress in turbulent flows, provided the thermal boundary layer generated by the heated film is completely submerged within the viscous sublayer of the turbulent boundary layer. It has been utilized by, among others, Ludwieg (1950), Liepmann & Skinner (1954), Myers, Schauer & Eustis (1963), and Bellhouse & Schultz (1966).

Measurements of the periodic wall shear stress in pulsatile turbulent pipe flow using

† Current address: Department of Mechanical Engineering, Washington State University, Pullman, Washington 99164-2920.

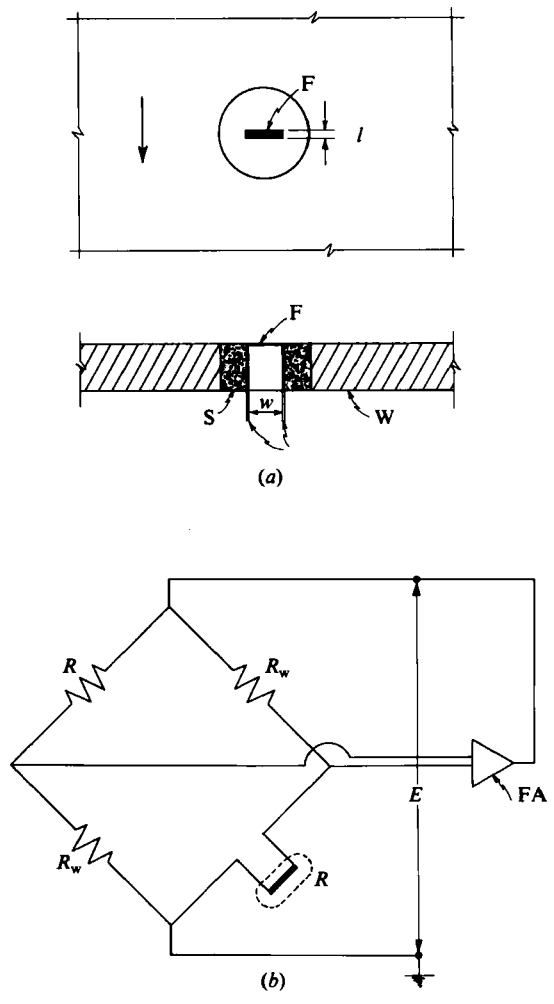

FIGURE 1. Schematic sketch of the hot-film and the bridge circuit. (*a*) Hot-film construction: F, film; S, substrate; W, wall; arrow indicates the direction of flow, l and w indicate the length and width of the film. (*b*) Anemometer bridge circuit: R, operating resistance of the film; R_w fixed resistance; FA, high-gain feedback amplifier; E, bridge output voltage.

a hot-film gauge were reported by Tu & Ramaprian (1983). However, the simple relation between wall shear stress and heat-transfer rate given by (1) may break down in unsteady flows, as first noticed by Bellhouse & Schultz (1966). In the particularly important case of oscillatory flows, breakdown can be expected to occur at 'high' frequencies of oscillation. Pedley (1972) presented an analysis, based on asymptotic techniques, to determine the unsteady response of wall heat transfer in oscillatory laminar flow. This is useful in establishing the conditions under which significant departures from a quasi-steady behaviour occur, leading to the breakdown of (1). An extension of this work (Pedley 1976) deals with reverse-flow situations. Kaiping (1983) avoided some of Pedley's simplifying assumptions by resorting to numerical techniques. He presented graphs from which departures from a quasi-steady response can be quantified for given amplitudes and frequencies of oscillation. These studies, however, do not deal with the problem of generalising (1) to include unsteady flows. An attempt in this direction was made by Bellhouse & Schultz (1966). Their interest

was in the estimation of the frequency spectrum of wall-shear-stress fluctuations from measurements of the instantaneous rate of wall-heat transfer. Hence, they obtained experimentally the actual relationship between the amplitude of oscillation of the wall shear stress and that of the heat-transfer rate, as a function of the frequency, from a calibration experiment in the periodic laminar boundary layer on a longitudinally oscillating flat plate. The amplitude of oscillation of the wall shear stress can be calculated analytically in this case. However, because of practical limitations, these calibration experiments could not be extended to higher frequencies. It therefore became necessary for them to extrapolate the results from the lower-frequency calibration experiments in order to estimate the higher-frequency end of the spectrum of wall-shear-stress fluctuations. They did not develop an appropriate theory for unsteady flows, however.

In this paper, a theory is presented for the measurement of skin friction in unsteady flows, using hot-film gauges. This theory has lead to a formula more general than (1). The accuracy of the new formula is demonstrated for the case of laminar and turbulent boundary-layer flows subjected to a periodic free-stream velocity U_e of the form

$$U_e(t) = U_0(1 + \epsilon \sin \omega t). \tag{2}$$

where ω is the angular frequency of oscillation, U_0 the time-mean velocity and ϵ the relative amplitude of oscillation. This is accomplished by comparing the instantaneous (ensemble-averaged) wall shear stress obtained from the new formula against exact numerical solutions of the governing partial differential equations. In addition, the failure of (1) at relatively high frequencies is also shown. The proposed formula is thus expected to widen the range of application of the hot-film gauge to include many unsteady-flow situations.

2. Development of a general formula

The problem under study is shown schematically in figure 2. A thermal boundary layer develops within a laminar or turbulent hydrodynamic boundary layer over the heated film of (effective) length L in the streamwise direction. The thermal boundary layer is produced by a sudden jump in the surface temperature, from a constant value equal to the ambient temperature T_e to the higher constant value T_0, at the location $x = x_0$. In the case of a turbulent boundary layer it is assumed that the thermal boundary layer is completely submerged within the viscous sublayer, so that any effect of turbulent diffusion can be neglected. We then seek a relationship between the local skin friction τ_w and heat-transfer rate Q_w from the fluid to the wall. We shall follow a procedure similar to the one outlined by Bellhouse & Schultz (1966), conveniently generalized to deal with unsteady-flow situations. The equation governing the temperature distribution T is

$$\frac{\partial T}{\partial t} + U\frac{\partial T}{\partial x} + V\frac{\partial T}{\partial y} = \frac{k}{\rho c_p}\frac{\partial^2 T}{\partial y^2} \tag{3}$$

where r is the time, U and V are the velocity components along the x and y axes respectively, and ρ, k and c_p are the mass density, thermal conductivity and specific heat of the fluid, respectively. In (3) we have neglected viscous dissipation, and considered the flow to be two-dimensional. For the sake of clarity the theory will first

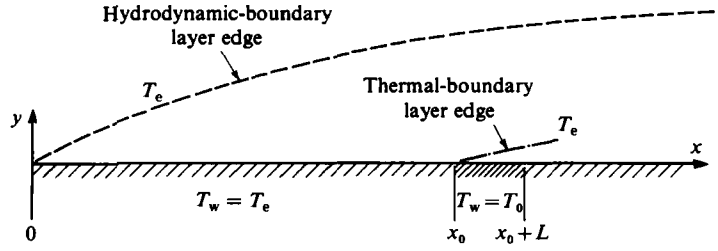

FIGURE 2. Definition of the problem.

be developed for laminar flow. It can easily be extended to turbulent flows later. Using the continuity equation,

$$\frac{\partial U}{\partial x}+\frac{\partial V}{\partial y}=0, \tag{4}$$

(3) can be rewritten as

$$\frac{\partial T}{\partial t}+\frac{\partial}{\partial x}(UT)+\frac{\partial}{\partial y}(VT)=\frac{k}{\rho c_p}\frac{\partial^2 T}{\partial y^2}. \tag{5}$$

Integrating (4) across the thermal boundary layer up to a point $y = y_e$, which is beyond the edge of this layer, we obtain

$$\frac{\partial}{\partial x}\int_0^{y_e} U\,dy+V_e=0, \tag{6}$$

where V_e is the velocity at $y = y_e$. Noting further that $T = T_e$ at $y = y_e$, we obtain from (5)

$$\frac{\partial}{\partial t}\int_0^{y_e} T\,dy+\frac{\partial}{\partial x}\int_0^{y_e} UT\,dy+V_e T_e=-\frac{1}{\rho c_p}Q_w. \tag{7}$$

Combining (6) and (7) we get

$$\frac{\partial}{\partial t}\int_0^{y_e}(T-T_e)\,dy+\frac{\partial}{\partial x}\int_0^{y_e} U(T-T_e)\,dy=-\frac{1}{\rho c_p}Q_w. \tag{8}$$

Now we shall introduce a key assumption regarding the velocity profile. Considering that, in the region where the thermal boundary layer exists, inertia effects can be ignored, the velocity profile can be approximated by

$$U=\frac{\tau_w}{\mu}y+\frac{1}{2\mu}\left(\frac{\partial p}{\partial x}\right)y^2, \tag{9}$$

where p is the pressure and μ is the viscosity of the fluid. The implications of this hypothesis (one of the classical hypothesis in the theory for hot-film gauges) will be discussed later. For the time being it sufficies to say that the restrictions for this assumption to apply are met in most practical applications. Introducing (9) into (8) we obtain

$$\mu\frac{\partial}{\partial t}\int_0^{y_e}(T-T_e)\,dy+\frac{\partial}{\partial x}\left[\tau_w\int_0^{y_e} y(T-T_e)\,dy+\frac{1}{2}\left(\frac{\partial p}{\partial x}\right)\int_0^{y_e} y^2(T-T_e)\,dy\right]=-\frac{\mu}{\rho c_p}Q_w. \tag{10}$$

We now assume that temperature distributions in the thermal boundary layer are self-similar at any instant of time. Thus, one can write

$$\frac{T-T_e}{T_w-T_e} = f(\xi, t), \tag{11}$$

where

$$\xi = \frac{y}{\delta_T(x,t)}, \tag{12}$$

and δ_T is the local thermal-boundary-layer thickness. Note that, as a consequence, the 'shape parameter'

$$\lambda(t) = \frac{Q_w \delta_T}{k(T_w-T_e)} = \left.\frac{\partial f}{\partial \xi}\right|_{\xi=0} \tag{13}$$

must be a constant for the flow, for each instant of time. In addition, we define three more 'shape parameters', namely

$$c(t) \equiv -\lambda \int_0^1 f(\xi, t)\,\mathrm{d}\xi, \tag{14}$$

$$a(t) \equiv \lambda^2 \int_0^1 \xi f(\xi, t)\,\mathrm{d}\xi, \tag{15}$$

$$b(t) \equiv -\lambda^3 \int_0^1 \xi^2 f(\xi, t)\,\mathrm{d}\xi, \tag{16}$$

where the integration can be truncated at $\xi = 1$ since it is assumed that $T \simeq T_e$ for $y > \delta_T$. Introducing (11)–(16) into (10) we obtain

$$-\frac{\partial}{\partial t}\left[\frac{c\mu k(T_w-T_e)^2}{Q_w}\right] + \frac{\partial}{\partial x}\left[\frac{ak^2(T_w-T_e)^3\tau_w}{Q_w^2} - \frac{bk^3(T_w-T_e)^4}{2Q_w^3}\left(\frac{\partial p}{\partial x}\right)\right] = -\frac{\mu Q_w}{\rho c_p}. \tag{17}$$

The last step consists of integrating (17) along the surface from some point $x = x_1$, such that $x_1 < x_0$, to $x = x_0 + L$ (see figure 2). We then obtain

$$-\frac{\partial}{\partial t}\left[c\mu k\Delta T_0^2 \int_{x_0}^{x_0+L} \frac{\mathrm{d}x}{Q_w(x,t)}\right] + ak^2\Delta T_0^3 \frac{\tau_{wL}}{Q_{wL}^2} - \frac{bk^3\Delta T_0^4}{2Q_{wL}^3}\left(\frac{\partial p}{\partial x}\right)_L = -\frac{\mu}{\rho c_p}\int_{x_0}^{x_0+L} Q_w(x,t)\,\mathrm{d}x, \tag{18}$$

where $\Delta T_0 = T_0 - T_e$, and the subscript L refers to values at $x = x_0 + L$. In the above integration we have assumed that λ, defined in (13), remains finite even for $T_w \to T_e$. This makes the contributions from $x = x_1$ to $x = x_0$ to vanish. To evaluate the remaining integrals in (18) we shall further assume an expression for δ_T of the form

$$\frac{\delta_T(x,t)}{\delta_T(x_0+L,t)} = \left[\frac{x-x_0}{L}\right]^n, \tag{19}$$

where n is an unknown exponent and can, in general, depend on time. Equation (19) is a relatively weak hypothesis. Moreover, a relation like this, with $n = \frac{1}{3}$, holds approximately for steady laminar flow when $L \ll x_0$ (see Kays & Crawford 1980). Using (13) and (19) we can obtain, after some algebra, the following results (see Menendez & Ramaprian 1984*b*):

$$\tau_{wL} = -\frac{\mu L}{(1-n)a\rho c_p k^2}\left(\frac{Q_{wL}}{\Delta T_0}\right)^3 + \frac{bk}{2a}\left(\frac{\partial p}{\partial x}\right)_L\left(\frac{\Delta T_0}{Q_{wL}}\right) + \frac{\mu L}{ak}\frac{Q_{wL}^2}{\Delta T_0}\frac{\partial}{\partial t}\left[\frac{c}{(1+n)Q_{wL}}\right]. \tag{20}$$

For steady flow $\partial/\partial t = 0$, (20) reduces to that presented by Bellhouse & Schultz (1966), except for the corrective factor $1/(1-n)$. Finally, assuming that c and n are independent of time, and considering the particular free-stream-velocity distribution given by (2), which means that

$$\left(\frac{\partial p}{\partial x}\right)_L = -\rho\left(\frac{\mathrm{d}U_e}{\mathrm{d}t}\right)_L = -\rho\epsilon\omega U_0 \cos\omega t, \tag{21}$$

(20) can be rewritten in the following simplified form

$$\tau_{wL} = -\left(A_1 Q_{wL}^3 + A_2 \frac{\cos\omega t}{Q_w L} + A_3 \frac{\partial Q_{wL}}{\partial t}\right), \tag{22}$$

where

$$A_1 \equiv \frac{\mu L}{(1-n)\, a\rho c_p\, k^2 (\Delta T_0)^3}, \tag{23}$$

$$A_2 \equiv \frac{bk(\Delta T_0)\, a\rho\epsilon\omega U_0}{2a}, \tag{24}$$

$$A_3 \equiv \frac{\mu L c}{(1+n)\, ak(\Delta T_0)}. \tag{25}$$

Equation (22) has been developed for laminar flows. It can also be regarded as the relationship between the instantaneous values of wall shear stress and wall heat flux in turbulent flows. Taking the ensemble averages of (22) over a large number of cycles, one then gets

$$\langle \tau_w \rangle = -A_1 \langle Q_{\omega L}^3 \rangle + A_2 \left\langle \left\{ \frac{1}{Q_{\omega L}} \right\} \right\rangle \cos\omega t + A_3 \frac{\partial}{\partial t} \langle Q_{\omega L} \rangle. \tag{26}$$

If the turbulent fluctuations in $\langle \tau_w \rangle$ and $\langle Q_{\omega L} \rangle$ are assumed to be 'small' compared with their ensemble averaged values, (26) can be linearized to yield

$$\langle \tau_w \rangle = -A_1 \{\langle Q_{\omega L} \rangle\}^3 + \frac{A_2}{\langle Q_{\omega L} \rangle} \cos\omega t + A_3 \frac{\partial}{\partial t} \langle Q_{\omega L} \rangle. \tag{27}$$

The shape parameters a, b and c and the shape exponent n can, in general, be functions of time in unsteady flow. However, finite-difference solutions of the governing equations (to be discussed in §3) indicated that a, b, c and n, in general, vary insignificantly during a cycle in the periodic boundary layer. For most operating conditions it was found to be adequate to treat them as 'universal' constants and use the following average values for steady as well as unsteady flows.

$$\left.\begin{aligned} &a = 0.23, \quad b = 0.14, \quad c = 0.56 \\ &n = 0.29 \quad \text{for laminar flows,} \\ &n = 0.25 \quad \text{for turbulent flows.} \end{aligned}\right\} \tag{28}$$

While the above values were obtained for $L/x_0 \approx 0$ (which is typical of heat-flux-gauge operation) careful study indicates that these values vary only slightly in the range $0 \lesssim L/x_0 \lesssim 1$ (see Menendez & Ramaprian 1984*b*).

Equation (22) is the fundamental formula being proposed for obtaining skin friction from the wall heat-transfer rate. A version of the formula more convenient to use in practice is presented in §5. In the particular case of steady flow (in zero pressure gradient) (22) reduces to

$$\tau_{wL} = -A_1 Q_{wL}^3 \tag{29}$$

which is the classical formula proposed for hot-film measurements. Equation (22) is verified in the following section for the case $L/x \ll 1$, which corresponds to the measurement of wall shear stress using a hot-film gauge. The acceptability of the assumptions leading to (22) and the restrictions imposed by them are examined in the appendix.

3. Verification of the formula

3.1. *Method of calculation*

To test the accuracy of (22), a finite-difference procedure was used to calculate the wall shear stress and wall heat-transfer rate in a periodic boundary layer with a free-stream-velocity variation described by (2). First, the hydrodynamic equations for the boundary layer (continuity and momentum) were solved. This provided the cyclical variation of the wall shear stress τ_w, and the distributions of U and V which drive the unsteady thermal boundary layer. Next, the unsteady (laminar) thermal-boundary-layer equation was solved, from which the cyclical variations of the wall heat transfer rate Q_w was obtained.

The ensemble-averaged hydrodynamic-boundary-layer equations for an incompressible, two-dimensional, unsteady, turbulent flow are:

$$\frac{\partial \langle U \rangle}{\partial x} + \frac{\partial \langle V \rangle}{\partial y} = 0; \tag{30}$$

$$\frac{\partial \langle U \rangle}{\partial t} + \langle U \rangle \frac{\partial \langle U \rangle}{\partial x} + \langle V \rangle \frac{\partial \langle U \rangle}{\partial y} = -\frac{1}{\rho}\frac{\partial \langle p \rangle}{\partial x} + \nu \frac{\partial^2 \langle U \rangle}{\partial y^2} - \frac{\partial}{\partial y}\langle uv \rangle; \tag{31}$$

where ν is the kinematic viscosity of the fluid. The last term on the right-hand side of (31) represents turbulent diffusion; u and v are the turbulent fluctuations of U and V, respectively, and $-\langle uv \rangle$ is the ensemble-averaged Reynolds shear stress, which needs to be modelled in order for the system of equations to be closed. Equations (30) and (31) were solved using a finite-difference method, details of which are described in Menendez & Ramaprian (1982, 1984*a*). In this method, the equations are solved in primitive variables $\langle U \rangle$ and $\langle V \rangle$. The x-coordinate is non-dimensionalized as

$$\tilde{X} = \frac{\omega x}{U_0}, \tag{32}$$

which can be interpreted as a frequency parameter that measures the importance of unsteadiness relative to convection. The y-coordinate is normalized using a lengthscale representative of the hydrodynamic-boundary-layer thickness. Two important features of this calculation procedure are that it retains numerical accuracy even at very high frequencies and it can handle reversals of flow (not flow separation) during the oscillation cycle.

The thermal-boundary-layer equation (3) was solved next. The same numerical procedure was used as that employed to solve the hydrodynamic equations. In this case the x-coordinate was non-dimensionalized as

$$\tilde{x} = \frac{\omega(x - x_0)}{U_*} \tag{33}$$

where U_* (a constant) is the scale for the longitudinal velocity within the thermal layer. Note that $\tilde{x}$ can also be interpreted as a second frequency parameter, measuring the importance of unsteadiness relative to convection in the thermal boundary layer.

$\tilde{X}_0$	ϵ	$\tilde{L}$	Case
0.01	0.50	0.0005	L1A
		0.01	L1B
0.1	0.50	0.05	L2
0.5	0.50	0.10	L3
1.0	0.50	0.05	L4A
	0.30	0.10	L4B
2.0	0.50	0.10	L5A
	0.25	0.10	L5B
5.0	0.50	0.30	L6A
	0.15	0.10	L6B
10.0	0.10	0.10	L7

TABLE 1. Selected values of $\tilde{X}_0$, ϵ and $\tilde{L}$ for unsteady-laminar-flow cases

The restriction $L \ll x_0$ was explicitly used by assuming that the calculated velocity profiles for $\langle U \rangle$ and $\langle V \rangle$ were invariant with $\tilde{x}$ along the hot film. More details on the calculation procedure for the thermal boundary layer equation are presented in Menendez & Ramaprian (1984*b*).

Calculations were made for laminar as well as turbulent flows. In the laminar-flow calculations $\langle uv \rangle$ was set equal to zero. In the turbulent-flow calculations a one-equation model, the so called Prandtl energy model (see Acharya & Reynolds 1975; Menendez & Ramaprian 1982), was used to describe $\langle uv \rangle$. It is possible that the calculated velocity field may be somewhat sensitive to the specific turbulence model used. However, since our interest is to study the relation between wall shear stress and wall heat-transfer rate, and since the temperature distribution is driven by the calculated velocity distribution, it is necessary for the velocity distribution to be only *representative* of the actual velocity distribution. The thermal-boundary-layer calculations are exact since they do not involve any turbulence modelling.

By appropriately rewriting (22) it can be shown that the relationship between wall shear stress and wall heat flux depends on the frequency parameter $\tilde{x}_0$, the non-dimensional effective film length $\tilde{L} = \omega L/U^*$, the relative amplitude ϵ, the mean-flow Reynolds number $(U_0 x_0/\nu)$ and the Prandtl number Pr of the fluid. The calculations were made for a Prandtl number of 7, being the value for water at a temperature of 20 °C. The calculations were repeated for several combinations of values of $\tilde{X}_0$, ϵ and $\tilde{L}$. It is important to realize that these cannot be chosen arbitrarily, if the restrictions leading to (22) are to be satisfied. These restrictions are discussed in the Appendix. It can be mentioned here however that, for the selected values of $\tilde{X}_0$ and ϵ, the largest permissible values of $\tilde{L}$ were taken in order to obtain maximum effects of unsteadiness. Both laminar and turbulent flows were considered. Turbulent-flow calculations were performed for a typical mean-flow Reynolds number of 2×10^6. In the case of laminar flows the solutions were made independent of Reynolds number by appropriately stretching the coordinates. The results for laminar and turbulent flows are separately discussed below.

3.2. *Results for laminar flow*

Several unsteady-laminar-flow calculations were performed. These varied from very low ($\tilde{X}_0 \ll 1$) to very high frequencies ($\tilde{X}_0 \gg 1$). Table 1 shows the selected values of the parameters $\tilde{X}_0$, ϵ and $\tilde{L}$ for the different cases. The velocity scale U_* was chosen as $0.291 U_0$, which roughly corresponds to a velocity value at the outer edge of the thermal boundary layer for the cases studied. The results of the calculation are

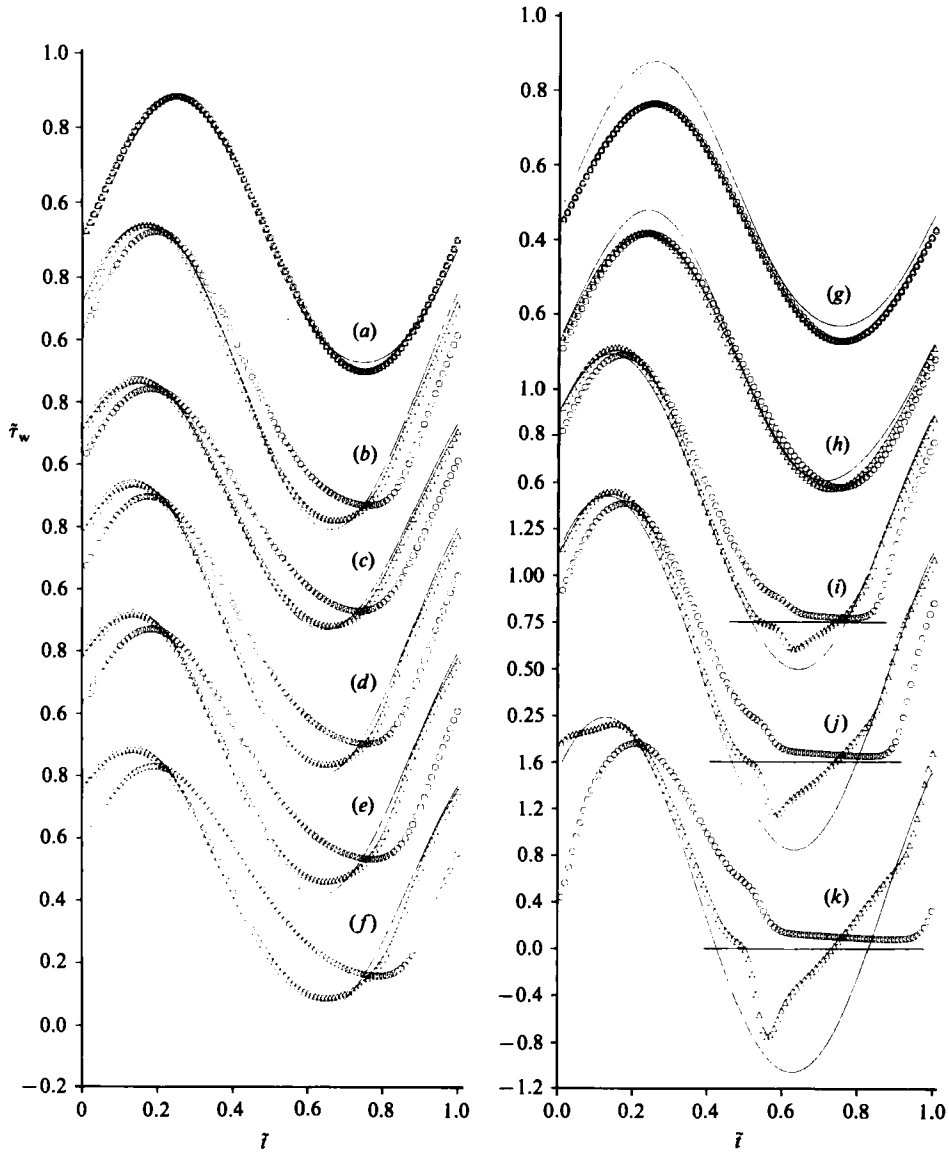

FIGURE 3. Variation of the wall shear stress during the oscillation cycle for laminar flow: (*a*) case L1A; (*b*) L3; (*c*) L4B; (*d*) L5B; (*e*) L6B; (*f*) L7; (*g*) L1B; (*h*) L2; (*i*) L4A; (*j*) L5A; (*k*) L6A; ——, exact solution, ○, conventional method; △, present method.

presented in figure 3 in a Reynolds-number-independent form using the following dimensionless coordinates:

$$\left.\begin{aligned} \tilde{\tau}_w &= \left(2\frac{U_0 x_0}{\nu}\right)^{\frac{1}{2}} \frac{\tau_{wL}}{\rho U_0^2}; \\ \tilde{t} &= \omega t. \end{aligned}\right\} \tag{34}$$

This figure shows the variation of the wall shear stress during the oscillation cycle. Results obtained from three different methods are compared. These methods are:

(i) directly from the hydrodynamic solution (i.e. from the velocity profile), which we shall refer to as the 'exact' solution;

(ii) from the use of (29), in which (the exact) Q_{wL} is obtained from the numerical solution of the thermal-boundary-layer equation. We shall refer to this as the 'conventional' method;

(iii) from the same procedure as (ii), except that the modified relationship (22) is used in place of the conventional relationship (29). We shall refer to this as the 'present' method.

Figure 3 (*a*) shows the results for case L1A. Not much difference is observed between the different calculations in this case. Actually, they agree within the range of numerical errors. This was to be expected at the very low value of the frequency parameter $\tilde{L}$ for this flow.

The wall shear stress for case L3 is presented next, in figure 3 (*b*). This time, it is readily observed how the present method gives much better results than the conventional approach. In fact, the results for $\tilde{\tau}_w$ from the conventional method must be considered poor: its amplitude is too small and it lags behind the exact solution. This clearly illustrates the necessity of using the present method when $\tilde{L}$ is not very small. Similar results are obtained for cases L4B, L5B, L6B, and L7, as illustrated by figure 3 (*c*)–(*f*) respectively. Note that, for these runs, the selected values of ϵ (table 1) are smaller for larger $\tilde{X}_0$. This was done in order to avoid the occurrence of flow reversal (see below).

The results for cases L1B and L2 are shown in figure 3 (*g*) and (*h*), respectively. For these cases both the conventional and present results give poor agreement with the exact solution. The problem here seems to be associated with the fact that $\tilde{L}$ is of the order of x_0 (see table 1), violating one of the assumptions of the numerical procedure. Obviously, this case is not of interest in hot-film applications.

Cases L4A, L5A and L6A were selected in order to study the consequences of the occurrence of flow reversal during part of the cycle. Figure 3 (*i*)–(*k*) show the results obtained. It is observed that the conventional method gives results which are not even qualitatively correct over a significant part of the cycle. This it to be expected since wall heat flux does not reverse in direction even when the wall shear stress reverses. Hence the conventional method cannot give negative values of wall shear stress. In fact the analogy between heat and momentum transfer at the wall breaks down over a substantial part of the oscillation cycle. The present method is seen to perform much better in capturing the behaviour of the true wall shear stress. Even this method fails to describe *correctly* the variation in wall shear stress *during* flow reversal. However, during the remaining part of the cycle the present calculation still gives satisfactory results, except when the backflow is quite severe, as in figure 3 (*k*). It should be noted that cases L5A and L6A are extremely severe test cases and are unlikely to be encountered in practical situations involving the use of the hot-film gauge.

3.3. *Results for turbulent flow*

Calculations for turbulent flow were performed for a wide range of frequencies. The frequency regime was characterized according to the following criterion (Menendez & Ramaprian 1983):

$$\tilde{X}_0 \lesssim 1: \quad \text{low-frequency regime;}$$

$$1 \ll \tilde{X}_0 \lesssim R_*^{\frac{1}{2}}: \quad \text{intermediate-frequency regime;}$$

$$R_*^{\frac{1}{2}} \ll \tilde{X}_0 \ll R_*: \quad \text{high-frequency regime;}$$

$$R_* \lesssim \tilde{X}_0: \quad \text{very-high-frequency regime;}$$

$\tilde{X}_0$	ϵ	$\tilde{L}$	Case
0.01	0.50	10^{-5}	T1
1.0	0.50	10^{-3}	T2
10.0	0.40	0.01	T3
35.0	0.30	0.05	T4
350	0.10	0.50	T5
1350	0.05	0.10	T6

TABLE 2. Selected values of $\tilde{X}_0$, ϵ and $\tilde{L}$ for unsteady-turbulent-flow cases

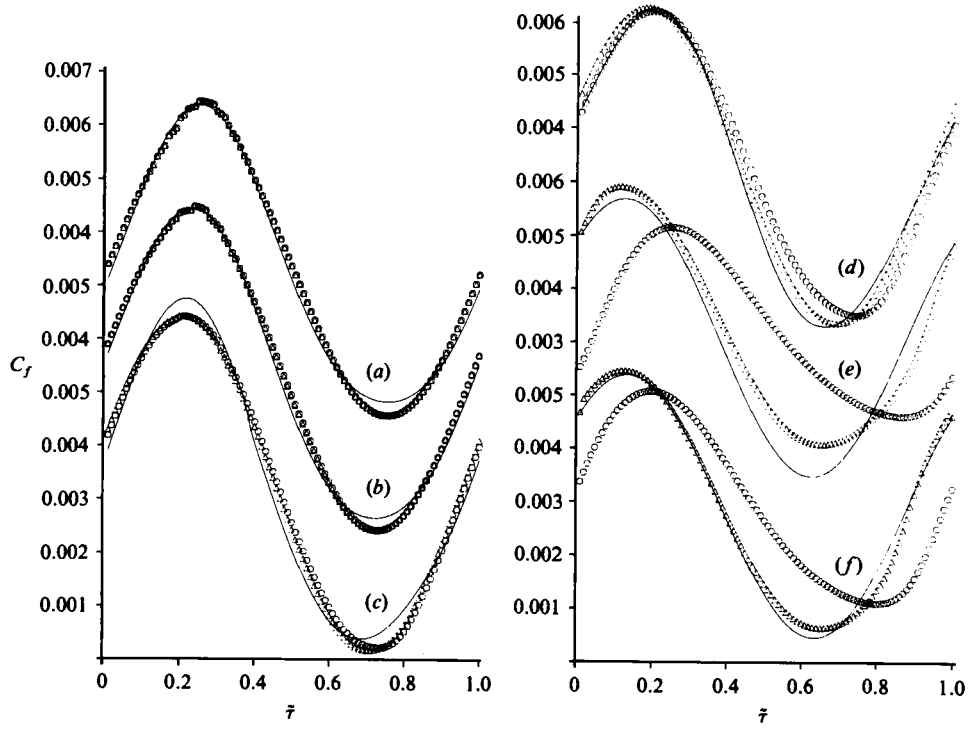

FIGURE 4. Variation of the skin friction coefficient during the oscillation cycle for turbulent flow: (*a*) Case T1; (*b*) T2; (*c*) T3; (*d*) T4; (*e*) T5; (*f*) T6; Symbols as in figure 3.

where $R_* = \bar{u}_* \bar{\delta}/\nu$; $\bar{u}_*$ is the mean shear velocity and $\bar{\delta}$ the mean hydrodynamic-boundary-layer thickness. Table 2 presents the selected values of $\tilde{x}_0$, ϵ and $\tilde{L}$. In all cases ϵ was taken as large as possible, but small enough to avoid flow reversal.

Figure 4 presents the results for the skin-friction coefficient $C_f = 2\tau_w/\rho U_0^2$ for the various test cases. Referring to figure 4(*a*), which shows the results for case T1, it is seen that there is good agreement between the exact values of $\langle C_f \rangle$ and those obtained from the conventional and present methods (which are nearly identical to each other owing to the small value of $\tilde{L}$). The results for cases T2 and T3 are similar to the previous ones, as shown in figures 4(*b*) and (*c*). The difference between the conventional and present methods, however, is more noticeable for case T3.

The value of $\tilde{L}$ is sufficiently large in case T4 for the effect of unsteadiness to become important. Figure 4(*d*) shows how the present method leads to a better estimation

of the phase of $\langle C_f \rangle$ than the conventional method. A Fourier analysis of the results shows that the first harmonic of $\langle C_f \rangle$ (which is, in fact, the most significant) obtained from the conventional method lags the exact solution by 9.21°, while the present method estimates the phase within 0.87° of the exact solution. Case T5, shown in figure 4(*e*), must be considered a rather extreme situation, unlikely to be encountered in hot-film usage, since $\tilde{L}$ is chosen to be unrealistically large. It is seen that the present method still represents a dramatic improvement over the conventional method, even in this extreme case. The amplitude of oscillation estimated by the present method is 8 % lower than the exact solution, while the conventional method gives the amplitude 35 % too low. More dramatic is the improvement in the estimation of the phase. The present method reduces the error from −60.36° to −9.55°. Less extreme is case T6 for which results are shown in figure 4(*f*). It is seen that the present method gives a very good prediction of both the amplitude and phase lag.

4. Practical considerations

A few more steps must now be taken to cast (22) into a form that is convenient for use in practice. Let us consider the more practical example of turbulent flows. Also, let us first examine the case of small fluctuations. To begin with, one should note that it is the total heat transfer $\langle Q_T \rangle$ from the entire element to the fluid that is measured, and not the local heat transfer $\langle Q_w \rangle$. They are related through the equation

$$\langle Q_T \rangle (t) = -W \int_{x_0}^{x_0+L} \langle Q_w \rangle (\xi, t)\, d\xi. \tag{35}$$

Introducing the assumptions (13) and (19), the right-hand side can be integrated to yield

$$\langle Q_T \rangle (t) = -\frac{WL\langle Q_{wL} \rangle}{(1-n)} \tag{36}$$

where W is the effective width of the film. Furthermore, $\langle Q_T \rangle$ is related to the voltage E read from the anemometer as (see figure 1)

$$\langle Q_T \rangle = \frac{\langle E \rangle^2 R}{(R+R_w)^2} - \langle Q_s \rangle, \tag{37}$$

where R_w is the fixed bridge resistance (= 50 Ω in DISA M01 anemometer), R is the operating film resistance, and $\langle Q_s \rangle$ is the heat lost to the substrate. Then, in the case of *steady flow* with *zero or negligible pressure gradient*, (22) can be rewritten, using (36) and (37), as

$$\langle \tau_w \rangle = \frac{(1-n)^2 \mu}{a \rho c_p k^2 L^2 W^3 \Delta T_0^3} \left[\frac{\langle E \rangle^2 R}{(R+R_w)^2} - \langle Q_s \rangle \right]^3 \tag{38}$$

Two problems arise with the use of (38) (Hanratty & Campbell 1980). First, $\langle Q_s \rangle$ is not known. Secondly, the effective area of the element can, in general, be greater than the actual film surface area, as some heat may be transferred to the fluid from the substrate. Hence, L and W are also not known. The common practice, however, is to assume that

$$\langle \tau_w \rangle^{\frac{1}{3}} = A\langle E \rangle^2 + B, \tag{39}$$

where A and B are constants that can be obtained from calibration in steady flow at different free-stream velocities. This procedure has been found to be satisfactory for the use of the film probe in steady flows with negligible pressure gradient, at least

over limited but useful range of Reynolds numbers. The fact that the calibration relation (39) is well supported by experiments in steady flow suggests that it is reasonable to assume that for a given probe, operated at a given value of ΔT_0 the effective length L, effective width W and heat loss Q_s are independent of E and hence of the free-stream velocity. Being guided by this evidence, we next make the somewhat drastic assumption that these are constant in unsteady flows as well and have the same values as in steady flow. However, in unsteady flow it is still necessary to account for the two extra terms in (22). The best way is perhaps, to rewrite (22) as

$$\langle \tau_w \rangle = (A\langle E\rangle^2 + B)^3 + \frac{c_1}{(A\langle E\rangle^2 + B)} \frac{\mathrm{d}U_e}{\mathrm{d}t} + c_2 A \frac{\mathrm{d}\langle E\rangle^2}{\mathrm{d}t}. \tag{40}$$

The best way of obtaining the additional constants c_1 and c_2 is to calibrate the probe in pulsatile laminar flow, a procedure similar to that employed by Bellhouse & Schultz (1966) (but now backed by a consistent theory). This procedure, however, is not generally practicable. Therefore, an alternative procedure is proposed below.

Combining (38) and (39), we can obtain the following relations:

$$A = \left[\frac{(1-n)^2 \mu}{a\rho c_p k^2 L^2}\right]^{\frac{1}{3}} \frac{R}{W\Delta T_0 (R+R_w)^2}; \tag{41}$$

$$\langle Q_s \rangle = -\frac{BR}{A(R+R_w)^2}. \tag{42}$$

Equation (42) can be used to calculate $\langle Q_s \rangle$ once the constants A and B are known from steady-flow calibration. But (41) has two unknowns: L and W. To obtain the extra relationship between L and W a rather complicated three-dimensional heat-transfer problem should be solved. Instead, it will simply be assumed that

$$\frac{L}{l} = \frac{W}{w} \equiv \Delta_*, \tag{43}$$

where l and w are the actual length and width of the film, respectively, and $\Delta_* > 1$. Introducing (43) into (41) we obtain

$$\Delta_* = \left\{\frac{(1-n)^2 \mu}{a\rho c_p k^2 l^2}\left[\frac{R}{w A \Delta T_0 (R+R_w)^2}\right]^3\right\}^{\frac{1}{5}}, \tag{44}$$

from which Δ_* can be computed. Then, comparing (40) with (22) the constants c_1 and c_2 can be expressed as

$$c_1 = \frac{b}{2a}\left[\frac{k\rho^2 \mu l \Delta_*}{a(1-n)c_p}\right]^{\frac{1}{3}}, \tag{45}$$

$$c_2 = \frac{c}{(1+n)}\left[\frac{(1-n)\rho c_p \mu^2 l^2 \Delta_*^2}{a^2 k}\right]^{\frac{1}{3}}. \tag{46}$$

The complete procedure is as follows. For given experimental conditions the fluid properties (ρ, μ, k, c_p) are known. The shape parameters a, b, c and the exponent n are obtained from (28). The constants A and B are determined by calibration in steady flow. The ratio Δ_* is calculated from (44). This allows the computation of the constants c_1 and c_2 from (45) and (46), respectively. Thus, if the variation of U_e and E with time are measured, the wall shear stress can be calculated from (40). This procedure is to be regarded as a suggestion at this time. In order to establish its reliability, it would be necessary to compare it with other independent techniques

of measuring wall shear stress in unsteady flows, as such techniques become available in the future.

The second and the third terms on the right-hand side of (40) represent the corrections to be applied to the conventional relationship, to account for the effect of unsteadiness. These corrections become negligible if these terms are small compared with the first term on the right-hand side. For a periodic flow oscillating sinusoidally at a frequency ω, this condition leads to

$$\frac{\omega c_1[U_e]}{|\tau_w|^{\frac{4}{3}}} \ll 1 \tag{47}$$

and

$$\frac{\omega c_2[\tau_w^{\frac{1}{3}}]}{|\tau_w|} \ll 1, \tag{48}$$

where [ ] and | | respectively denote the amplitude of oscillation and order of magnitude of the enclosed quantity.

So far, it has been assumed that turbulent fluctuations in τ_w and Q_T (and hence in E) are small compared to the ensemble averaged values. Sandborn (1979), however, recognized that, when the turbulent fluctuations in τ_w are large compared with $\langle\tau_w\rangle$, large errors can arise from the use of this linearized relation. In these cases, the full nonlinear version (26) must be used; correspondingly, (39) and (40) would have to be written in terms of instantaneous values, namely

$$\tau_w = AE^2 + B \tag{49}$$

and

$$\tau_w = (AE^2+B)^3 + c_1 \frac{dU_e}{dt}\frac{1}{AE^2+B} + c_2 A \frac{dE^2}{dt}. \tag{50}$$

A method for obtaining the calibration constants A and B relating the instantaneous values of τ_w and E in (49) has been discussed by Ramaprian & Tu (1983). Once A and B are known, the instantaneous value of τ_w can be obtained from the instantaneous value of E using (50). The instantaneous values of E should be obtained from a suitable data-acquisition device. The instantaneous values of τ_w are then ensemble averaged to obtain $\langle\tau_w\rangle$.

Finally, it is important to note that the formulation represented by (40) is valid even in the presence of a non-negligible spatial-pressure gradient, provided one writes

$$\frac{dU_e}{dt} = \frac{\partial U_e}{\partial t} + U_e \frac{\partial U_e}{\partial x} \tag{51}$$

in (40). However, extra restrictions may appear in addition to those for zero time-mean pressure-gradient flow, if the second term on the right-hand side of (51) is much larger than the first term. These restrictions can be studied using a procedure analogous to that presented in the Appendix.

5. Application to the calculation of the turbulent spectral density

The present method, developed for the measurement of ensemble-averaged wall shear stress in periodic boundary layers, can be also applied to the estimation of the response of the hot-film gauge to the turbulent fluctuations of wall shear stress in *steady* flow. Let us rewrite the instantaneous relationship (22) in the following form

$$\tau_{wL} = -\left(A_1 Q_{wL}^3 + \frac{B_1}{Q_{wL}}\frac{dU_e}{dt} + A_3 \frac{\partial Q_{wL}}{\partial t}\right), \tag{52}$$

where

$$B_1 = \frac{b\rho k \Delta T_0}{2a}. \tag{53}$$

We now write

$$\left.\begin{aligned} \tau_{wL} &= \bar{\tau}_w + \Delta\tau_w, \\ Q_w &= \bar{Q}_w + \Delta Q_w, \\ U_e &= \bar{U}_e + \Delta U_e, \end{aligned}\right\} \tag{54}$$

where the overbar denotes time-mean quantities, and the symbol Δ now stands for the perturbation from the time-mean value due to a frequency 'f' in the turbulent spectrum. For illustration let us once again assume that the turbulent fluctuations are small compared to the time-mean quantities, then $\bar{\tau}_w$ and $\bar{Q}_w$ satisfy (29), while their fluctuations are related by

$$\Delta\tau_w \approx -\left[A_1 3\bar{Q}_w^2 \Delta Q_w + \frac{B_1}{\bar{Q}_w}\frac{d\Delta U_e}{dt} + A_3 \frac{\partial \Delta Q_w}{\partial t}\right]. \tag{55}$$

For the chosen frequency, we can write

$$\left.\begin{aligned} \Delta\tau_w &= \tau_{w1} e^{i\omega t}, \\ \Delta Q_w &= Q_{w1} e^{i\omega t}, \end{aligned}\right\} \tag{56}$$

where $\omega = 2\pi f$. The perturbation ΔU_e of the free-stream velocity can be neglected in this case, if the free stream is assumed to be non-turbulent. Introducing (56) into (55) we obtain

$$\tau_{w1} = -[A_1 3\bar{Q}_w^2 + iA_3\omega] Q_{w1}. \tag{57}$$

Equation (57) relates the wall-shear-stress fluctuations to wall-heat-transfer fluctuations in steady turbulent flow. It can be rewritten, in a more compact form, as

$$\tau_{w1} = -3A_1 \bar{Q}_w^2 Q_{w1} \Lambda, \tag{58}$$

where

$$\Lambda = 1 + i\frac{A_3\omega}{3A_1\bar{Q}_w^2} \tag{59}$$

is the response function. Using the relation (29) between the time-mean quantities, (56) can also be written in the form

$$\frac{\tau_{w1}}{\bar{\tau}_w} = 3\frac{Q_{w1}}{\bar{Q}_w}\Lambda. \tag{60}$$

For $\omega \to 0$, $\Lambda \to 1$ and the fluctuation in τ_w is in phase with the fluctuation in Q_w, and the relative amplitudes of the two are related by the quasi-steady relation

$$\frac{\tau_{w1}}{\bar{\tau}_w} = 3\frac{Q_{w1}}{\bar{Q}_w}. \tag{61}$$

At higher frequencies, the two fluctuations are related to each other via the response function Λ which, using (23), (24) and (29), can be rewritten as

$$\Lambda = 1 + i\frac{f}{f_0}, \tag{62}$$

where

$$f_0 = \frac{3(1+n)}{2\pi c}(\bar{\tau}_w)^{\frac{2}{3}}\left[\frac{k^2 a}{(1-n)\rho c_p \mu^2 \Delta^2 l^2}\right]^{\frac{1}{3}}. \tag{63}$$

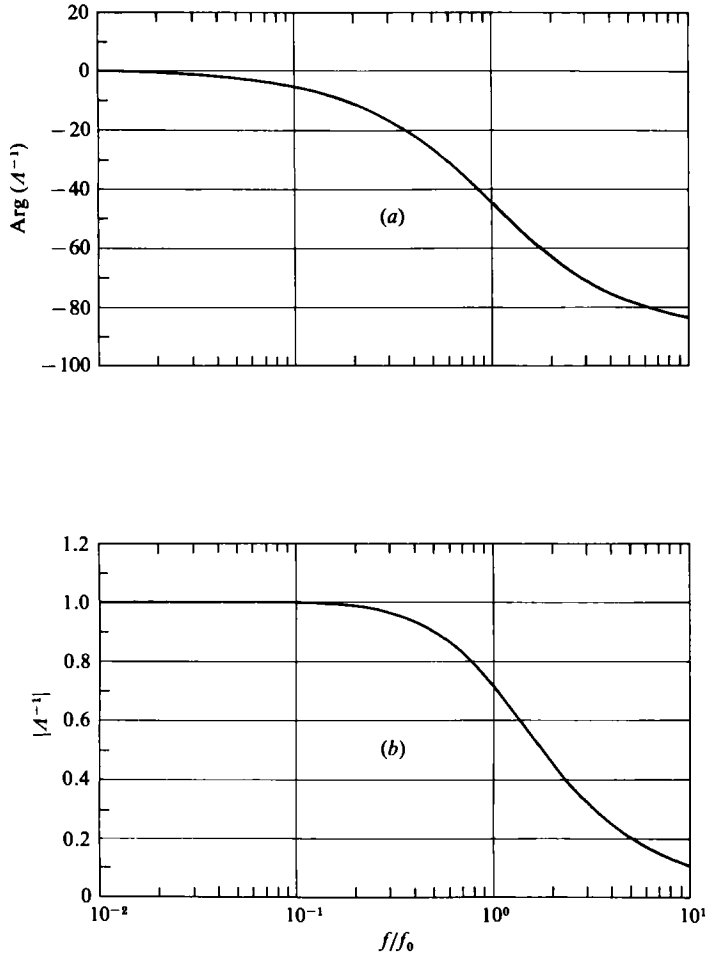

FIGURE 5. Relation between the heat-transfer-rate and shear-stress fluctuations at the wall in steady turbulent flow: (*a*) phase lag; (*b*) amplitude ratio.

Figure 5 shows the modulus and argument of A^{-1} as a function of f/f_0. Note that for $f = f_0$, the amplitude of the heat-transfer fluctuation is only 71 % of its quasi-steady value, and lags the wall shear stress fluctuation by 45°.

A typical wall-shear-stress energy spectrum, measured by the authors in the flat-plate boundary layer in a water tunnel, is shown in figure 6. This spectrum corresponds to the following time-mean conditions: $\overline{U} \simeq 90$ cm/s, $C_f \simeq 0.00329$. The wall shear stress was measured using a TSI 1237W flush-mounted hot-film probe and a DISA 55M01 constant-temperature anemometer. The film was maintained at an overheat ratio (T_0/T_e) of 1.1. The value of A_* for the probe under these conditions was determined to be 1.3 from (44), following the procedure described in §4. The spectrum was obtained by using the fast-Fourier-transform (FFT) technique on the sampled data. The anemometer output-voltage signal was low-pass filtered at 100 Hz and sampled and digitized at the rate of 200 samples per s. A total of 1024 consecutive samples we used in the FFT. The results shown in figure 6 were obtained by smoothing out an average of 80 spectra. The spectral results obtained from (60) are compared with those obtained from the quasi-steady relation (61). Only the spectral range (10–100 Hz) of relevance to the comparison is shown in the figure. Though the energy

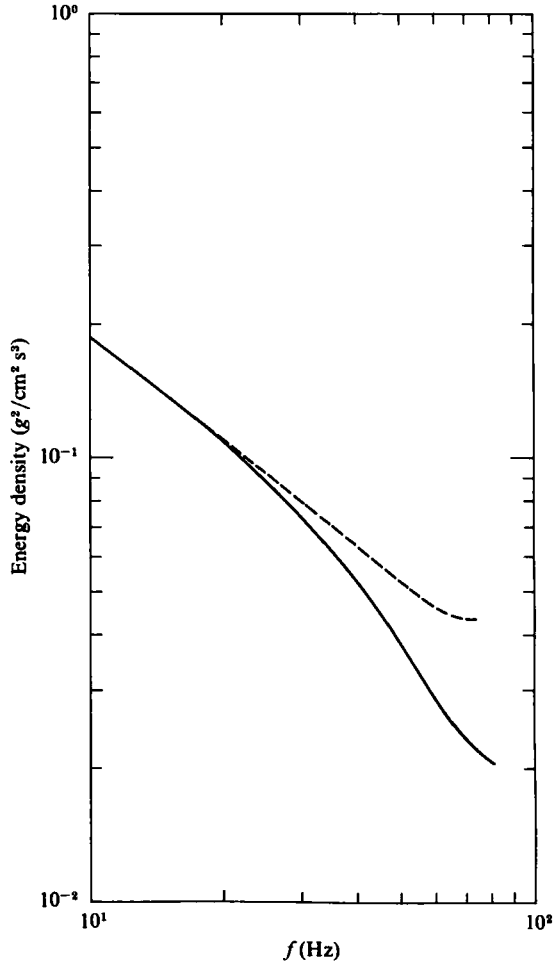

FIGURE 6. Measured energy spectrum of wall-shear-stress fluctuations in a flat-plate turbulent boundary layer: ——, conventional (quasi-steady) method (61); – – – –, present method (60).

content within this range is relatively small, it is seen that the present theory allows one to recover substantial information on the details of the spectrum that would otherwise have been lost. It is necessary to mention here that nonlinear effects due to large-amplitude turbulent fluctuations may modify the results of this illustrative example. The full nonlinear version of this theory would have to be used in such cases. The example selected here, however, is adequate to show that the present theory extends the realm of application of the hot-film gauge for wall-shear-stress measurement in turbulent flows. Unfortunately, direct verification of the accuracy of these spectral estimates is not possible till an independent instrumentation of known dynamic response is available for wall-shear-stress measurement in turbulent flows. Some recent and current developments using laser anemometry for wall-shear-stress and near-wall-flow measurements are likely to change this situation in the future.

Finally, it must be pointed out that, through (37), it has been assumed that the output voltage of the anemometer responds instantaneously to the heat-transfer rate from the element. The frequency response of present-day hot-film anemometers is generally good enough to justify this assumption. In fact, the present formula (60) is likely to break down at lower frequencies than those at which the electronic response becomes an issue.

6. Conclusions

The conventional calibration procedure for the flush-mounted hot film, when used as a skin-friction gauge, fails in high-frequency periodic flows. A theory for the use of this gauge in unsteady flows has been developed. This theory leads to the general formula (22), which replaces the conventional calibration formula (29). The usefulness and limitations of the proposed formula for laminar as well as turbulent flows have been established by comparing its accuracy against exact numerical solutions of the unsteady thermal and hydrodynamic boundary layers over the film.

Equations (40) and (50) represent the practical versions of the formula suitable for use in flow measurements. The present theory has been developed under certain restrictive assumptions. The constraints implied by these assumptions are described by (A 1), (A 9), (A 10), (A 11) and (A 14) of the Appendix. While the wide range of examples discussed in the paper shows that these assumptions are generally valid for most of the applications of the skin-friction gauge, it is necessary to verify that these five conditions are satisfied before applying the theory to any specific problem.

A procedure for the calibration of the probe for unsteady flow measurements is described.

A simplified linearized version of the formula (22) is presented in (60). This extends the use of the skin-friction gauge to the measurement of the energy spectrum of wall-shear-stress fluctuations in steady turbulent flows, in which such fluctuations are small relative to the mean value.

While the dynamic effects of heat transfer to the fluid have been fully taken into account in the present theory, a limitation of the present theory is that dynamic effects on the substrate heat transfer have been ignored, albeit with some justification. This aspect needs further theoretical study. It is also very important to conduct experiments that can lead to an assessment of the accuracy of the calibration procedure recommended in this paper. For example, this procedure can be tested by using it for measuring the instantaneous wall shear stress in a laminar periodic boundary layer, for which the exact solution can be obtained analytically or numerically. Unfortunately, because of experimental limitations, such tests could not be conducted by the authors. It is also possible to verify the accuracy of the present procedure if alternative independent techniques for measuring wall shear stress in unsteady turbulent flows become available in the future.

This work was supported by the U.S. Army Research Office, through their Grant/Contract No. DAAG-29-79-G-0017 and DAAG-29-83-K-0004.

Appendix. Restrictions of the theory presented

It is now necessary to establish the restrictive conditions under which the proposed formula (22) applies. These restrictions are imposed by some of the assumptions made in arriving at this formula. First, these assumptions are summarized below in the order they were introduced:

(i) The boundary-layer approximation is valid in the region of heat transfer.

(ii) Turbulent diffusion can be neglected in the thermal boundary layer.

(iii) The velocity profile within the thermal boundary layer can be approximated by (9).

(iv) The temperature profile is instantaneously self-similar.

(v) The thermal-boundary-layer thickness δ_T satisfies (19).

(vi) The shape parameters a, b, c and exponent n are independent of time.

(vii) $L \ll x_0$.

Assumption (i) implies that

$$\left(\frac{\delta_T}{L}\right)^2 \ll 1. \tag{A 1}$$

Assumption (ii) is only relevant for turbulent flows and relates to the fact that turbulent-energy diffusion has been neglected in (3). The mathematical consequence of this assumption is discussed together with the next assumption.

Assumption (iii) is one of the strongest assumptions. Hence, it has to be analysed in detail. The momentum equation for the hydrodynamic boundary layer in *laminar* flow is

$$\rho\left(\frac{\partial U}{\partial t}+U\frac{\partial U}{\partial x}+V\frac{\partial U}{\partial y}\right)=-\frac{\partial p}{\partial x}+\mu\frac{\partial^2 U}{\partial y^2}. \tag{A 2}$$

Double integration of (39) in the cross-stream direction, with the inertia terms neglected, yields (9), which is the velocity profile to zeroth order, $U^{(0)}$. The next order approximation $U^{(1)}$ can now be obtained, by adding to $U^{(0)}$ the contribution from the inertia terms, as

$$U^{(1)}(y) = U^{(0)}(y)+\frac{\rho}{\mu}\left\{\int_0^y \mathrm{d}y_1 \int_0^{y_1}\left[\frac{\partial U^{(0)}}{\partial t}(y_2)\right.\right.$$
$$\left.\left.+U^{(0)}(y_2)\frac{\partial U^{(0)}}{\partial x}(y_2)+V^{(0)}(y_2)\frac{\partial U^{(0)}}{\partial y_2}(y_2)\right]\mathrm{d}y_2\right\}, \tag{A 3}$$

where $V^{(0)}$ must be obtained from $U^{(0)}$ using (4), and where only the y-dependence is specified for economy of notation. Performing the above integration, we get

$$U^{(1)} = \frac{\tau_w}{\mu}y+\frac{1}{2\mu}\left(\frac{\partial p}{\partial x}\right)y^2+\frac{\rho}{6\mu^2}\frac{\partial \tau_w}{\partial t}y^3+\frac{\rho}{24\mu^2}\frac{\partial^2 p}{\partial t\,\partial x}y^4$$
$$+\frac{\rho}{24\mu^3}\tau_w\frac{\partial \tau_w}{\partial x}y^4+\frac{\rho}{60\mu^3}\tau_w\frac{\partial^2 p}{\partial x^2}y^5+\frac{\rho}{360\mu^3}\frac{\partial p}{\partial x}\frac{\partial^2 p}{\partial x^2}y^6. \tag{A 4}$$

Actually, (A 4) is accurate only up to terms of the order y^4. The correct higher-order approximation would result from applying (A 3) iteratively. However, we do not need to go that far. Assuming that the leading-order term of (A 4) is the first one, the zero-order solution will be a good representation of the velocity profile if the third, fourth and fifth terms on the right-hand side are very small compared with the first one. The order of magnitude of these terms in the thermal boundary layer is estimated as

$$\frac{\tau_w}{\mu}y \sim \frac{C_f U_0^2 \delta_T}{2\nu}, \tag{A 5}$$

$$\frac{\rho}{6\mu^2}\frac{\partial \tau_w}{\partial t}y^3 \sim \frac{C_f U_0^2 \omega\epsilon\delta_T^3}{6\nu^2}, \tag{A 6}$$

$$\frac{\rho}{24\mu^2}\frac{\partial^2 p}{\partial t\,\partial x}y^4 \sim \frac{U_0\omega^2\epsilon\delta_T^4}{24\nu^2}, \tag{A 7}$$

$$\frac{\rho}{24\mu^3}\tau_w\frac{\partial \tau_w}{\partial x}y^4 \sim \frac{C_f^2 U_0^4 \delta_T^4}{96\nu^3 x_0}, \tag{A 8}$$

where, in (A 6), it is assumed that the relative amplitude of oscillation of τ_w is twice the free-stream relative amplitude (a relation that holds, approximately, for quasi-steady flow), and C_f refers here to the order of magnitude of the skin-friction coefficient. The required conditions for assumption (iii) to be valid are, therefore,

$$\frac{\omega\delta_T^2}{\nu} \ll \frac{3}{\epsilon}, \tag{A 9}$$

$$\left(\frac{U_0\delta_T}{\nu}\right)\left(\frac{\omega\delta_T}{U_0}\right)^2 \ll 12\frac{C_f}{\epsilon}, \tag{A 10}$$

$$\left(\frac{U_0\delta_T}{\nu}\right)^2\left(\frac{\delta_T}{x_0}\right) \ll \frac{48}{C_f}. \tag{A 11}$$

In the case of *turbulent* flow, in addition to inertia, turbulent diffusion will give a small contribution to the velocity profile. To account for this effect, the introduction of a turbulence closure model is required. For our purpose, it is sufficient to consider a quasi-steady eddy-viscosity (μ_t) model, such as that given by White (1974), namely

$$\frac{\langle\mu_t\rangle}{\mu} = \frac{k^4}{6}\left(\frac{\langle u_*\rangle y}{\nu}\right)^3 \exp(-kB), \tag{A 12}$$

where $k \simeq 0.418$ and $B \simeq 5.5$ are the constants associated with the universal logarithmic velocity distribution. Double integration of the term $\partial/\partial y(\mu_t \partial U^{(0)}/\partial y)$ leads to the following additional term in (A 4):

$$\frac{k^4\rho^3}{24\mu^4}\langle\tau_w\rangle^{\frac{5}{2}} y^4 \exp(-kB) \sim 2.3\times10^{-5}\left[\frac{C_f^{\frac{5}{2}} U_0^5 \delta_T^4}{\nu^4}\right], \tag{A 13}$$

where the right-hand side gives the order of magnitude. Comparison with (A 5) leads to the condition

$$\left(\frac{U_0\delta_T}{\nu}\right)^3 \ll \frac{2\times10^4}{C_f^{\frac{3}{2}}}. \tag{A 14}$$

Equation (A 14) is the extra condition that must be satisfied in turbulent flow. It can be interpreted as the requirement that the thermal boundary layer is completely submerged in the viscous sublayer.

Assumption (viii), of course, introduces the restriction $\omega L/U_0 \ll \omega x_0/U_0$. The remaining assumptions do not seem to introduce any additional restrictions into the problem. In fact, exact numerical solutions showed that, in all the cases tested, these assumptions were valid. For more details, the reader is referred to Menendez & Ramaprian (1984*b*).

It is, however, necessary to ensure, before using the formula (40) or (50), that the conditions of operation of the hot-film gauge satisfy the restrictions implied by (A 1), (A 9)–(A 11) and (A 14). For this purpose, estimates for the thermal-boundary-layer thickness δ_T in laminar and turbulent flow are needed. The following are the suggested expressions that can be used as estimates (more details can be found in Menendez & Ramaprian 1984*b*):

$$\delta_T = \beta\left[\frac{(x-x_0)}{x_0}\right]^{\frac{1}{3}}\delta_e, \tag{A 15}$$

where δ_e (the hydrodynamic-boundary-layer thickness) and β are given by

$$\delta_e = 5\left(\frac{\nu x_0}{U_0}\right)^{\frac{1}{2}}; \quad \beta = \left(\frac{0.75}{Pr}\right)^{\frac{1}{3}} \tag{A 16}$$

for laminar flow, (see Kays & Crawford 1980) with Pr being the Prandtl number, and

$$\delta_e = 0.14 \frac{\nu}{U_0} \left(\frac{U_0 x_0}{\nu}\right)^{\frac{6}{7}}; \quad \beta = \left(\frac{0.057}{Pr}\right)^{\frac{1}{3}} \tag{A 17}$$

for turbulent flow (see White 1974). The expression for β is recommended by the authors in analogy with laminar flow. Present finite-difference calculations indicate that the numerical constant is 0.057 for water with a Prandtl number of 7.

REFERENCES

ACHARYA, M. & REYNOLDS, W. C. 1975 Measurements and predictions of a fully developed turbulent channel flow with imposed controlled oscillations. *Stanford University, Tech. Rep. TF-8.*

BELLHOUSE, B. J. & SCHULTZ, D. L. 1966 Determination of mean and dynamic skin friction, separation and transition in low-speed flow with a thin-film heated element. *J. Fluid Mech.* **24**, 379–400.

CURLE, N. 1962 *The Laminar Boundary Layer Equations.* Oxford University Press.

HANRATTY, T. J. & CAMPBELL, J. A. 1980 Measurement of wall shear stress. *Dept. of Chem. Engng, University of Illinois, Urbana, Illinois, Rep.*

KAIPING, P. 1983 Unsteady forced convective heat transfer from a hot film in non-reversing and reversing shear flow. *Trans. ASME* C: *J. Heat Transfer* **26**, 545–557.

KAYS, W. M. & CRAWFORD, M. E. 1980 *Convective Heat and Mass Transfer.* McGraw-Hill.

LIEPMANN, H. & SKINNER, G. 1954 Shearing-stress measurements by use of a heated element. *NACA TN No.* 3268.

LUDWIEG, H. 1950 Instruments for measuring the wall shearing stress of turbulent boundary layers. *NACA TM* 1284.

MENENDEZ, A. N. & RAMAPRIAN, B. R. 1982 Calculation of unsteady boundary layers. *IIHR Rep. No.* 248, The University of Iowa.

MENENDEZ, A. N. & RAMAPRIAN, B. R. 1983 Study of unsteady turbulent boundary layers. *IIHR Rep. No.* 270, The University of Iowa.

MENENDEZ, A. N. & RAMAPRIAN, B. R. 1984*a* Prediction of periodic boundary layers. *Intl J. Numer. Meth. Fluids* **4**, 781–800.

MENENDEZ, A. N. & RAMAPRIAN, B. R. 1984*b* On the measurement of skin friction in unsteady boundary layers using a flush-mounted hot-film gage. *IIHR Rep. No.* 272, The University of Iowa.

MYERS, G., SCHAUER, J. & EUSTIS, R. 1963 Plane turbulent wall jet flow development and friction factor. *Trans. ASME* D: *J. Basic Engng* **85**, 47.

PEDLEY, T. J. 1972 On the forced heat transfer from a hot film embedded in the wall in two dimensional unsteady flow. *J. Fluid Mech.* **55**, 329–357.

PEDLEY, T. J. 1976 Viscous boundary layers in reversing flow. *J. Fluid Mech.* **74**, 59–79.

RAMAPRIAN, B. R. & TU, S. W. 1983 Calibration of a heat flux gage for skin friction measurement. *Trans. ASME* I: *J. Fluids Engng* **105**, 455–457.

SANDBORN, V. A. 1979 Evaluation of the time-dependent surface shear stress in turbulent flows. *ASME Paper* 79-WA/FE-17.

TU, S. W. & RAMAPRIAN, B. R. 1983 Fully developed periodic turbulent pipe-flow. Part 1. Main experimental results and comparison with predictions. *J. Fluid Mech.* **137**, 31–58.

WHITE, F. M. 1974 *Viscous Fluid Flow.* McGraw-Hill.